IEEE Access
Multidisciplinary | Rapid Review | Open Access Journal

SPECIAL SECTION ON TRENDS, PERSPECTIVES AND PROSPECTS OF MACHINE LEARNING APPLIED TO BIOMEDICAL SYSTEMS IN INTERNET OF MEDICAL THINGS

Received August 6, 2018, accepted September 10, 2018, date of publication September 24, 2018, date of current version October 17, 2018.

Digital Object Identifier 10.1109/ACCESS.2018.2870950

Functional Assessment of Stenotic Coronary Artery in 3D Geometric Reconstruction From Fusion of Intravascular Ultrasound and X-Ray Angiography

XIAOQING WANG[1], CHANGNONG PENG[1], XIN LIU[2], AND ZHIGENG PAN[3]

[1]Department of Cardiology, Shenzhen Sun Yat-Sen Cardiovascular Hospital, Shenzhen 518055, China
[2]Shenzhen Institutes of Advanced Technology, Chinese Academy of Sciences, Shenzhen 518055, China
[3]Guangdong Industrial Institute of Virtual Reality, Foshan University, Foshan 528000, China

Corresponding author: Xin Liu (liu.xin@siat.ac.cn)

This work was supported in part by the National Key Research and Development Program of China under Grant 2016YFC1300300, in part by the Science and Technology Program of Shenzhen, China, under Grant JCYJ20170413114916687, and in part by the Shenzhen–Hong Kong Innovation Circle Program under Grant SGLH20161212104605195.

ABSTRACT We aimed to present an alternative method for calculating fractional flow reserve (FFR) from 3-D reconstruction of a coronary artery, based on coronary (X-ray) angiography and intravascular ultrasound (IVUS), to evaluate the ischemic-risk of stenosis and the relationship between FFR and geometrical features of the coronary lesion. The reconstruction of the 3-D catheter trajectory was obtained by the vertical intersection of spatial surfaces which were derived from the 2-D catheter curves in the angiography plane. Computational fluid dynamics was applied to calculate the hemodynamics in the coronary arteries and coronary flow-based FFR (fFFR) was obtained. Twenty-two stenotic coronary arteries were included in this paper for the evaluation of the proposed method. Good correlation between fFFR and the measured pressure wire-derived FFR was found ($F = 0.916$ and $P < 0.01$). Based on our computer modeling, the fFFR values correlated negatively with the severity of the stenosis ($r = -0.784$ and $P < 0.01$). However, fFFR had no significant correlation with coronary curvature, lesion length, and angle. Our method therefore provides a coronary vascular model-based means for computing FFR, and makes full use of the advantages of IVUS examination to diagnose the diseases.

INDEX TERMS Coronary angiography, intravascular ultrasound, 3-D reconstruction, fractional flow reserve (FFR), computational fluid dynamics (CFD), TIMI (thrombolysis in myocardial infarction).

I. INTRODUCTION

According to the Investigation Report on Heart Disease and Stroke Statistics—2017 Update [1], Cardiovascular Disease (CVD) is the most common underlying cause of death in the world, and Coronary Heart Disease (CHD) is the leading cause (45.1%) of deaths attributable to CVD [2]. Coronary (X-ray) Angiography (CAG), Intravascular Ultrasound (IVUS) and Fractional Flow Reserve (FFR) are commonly used for the diagnosis of CHD [3]–[5]. CAG is a procedure that involves placing a catheter in the coronary artery and use of contrast dye (usually containing iodine), which provides two-dimensional projection image of the coronary arteries for anatomic assessment of the presence and extent of stenosis. CAG had been considered a gold standard for obstructive disease and need for revascularization. However, the lack of three-dimensional information had limited the accuracy of CAG-based anatomic assessment. Intravascular ultrasound (IVUS) is a medical imaging methodology, involving the use of a specially designed catheter with a miniaturized ultrasound probe attached to the distal end of the catheter. The proximal end of the catheter is attached to the computerized ultrasound equipment. It allows the application of ultrasound technology (such as piezoelectric transducer) to obtain the anatomy of coronary arterial wall. IVUS is used to determine the plaque volume within the wall of the artery, wall thickness and the degree of stenosis of

the artery lumen [6]–[9]. Arguably the most valuable use of IVUS is to visualize coronary plaque, which is not available by using CAG along.

Functional assessment had been advanced by the development of fractional flow reserve (FFR) technology to provide physiological information of hemodynamic changes associated with coronary artery stenosis [10], [11]. FFR is recognized as the gold standard for the diagnosis of hemodynamic abnormalities caused by coronary artery stenosis [12]. FFR measurement involves determining the ratio between the hyperemic flow in a diseased coronary artery and the flow in a coronary artery without stenosis hypothetically [13]. FFR measurement is performed during routine coronary angiography by using a pressure wire to measure the coronary pressure in distal and proximal to a coronary artery stenosis under conditions of hyperemic state.

Clinical study indicated that threshold of FFR lower than 0.80 is generally considered to be associated with myocardial ischemia (MI)[FAME] and FFR < 0.75 was indication of myocardial ischemia. Despite the benefit for reducing usage of stent and risk of major adverse clinical events, the application of FFR was limited in clinical practice due to the invasive nature. Moreover, FFR is used only when it makes sense for medical follow up. When a patient has electrocardiography (ECG) changes and a 90 percent blockage, or a stress test reveals an inadequate blood supply, there is no need for FFR before proceeding with revascularization. Besides, FFR is not suitable for the assessment of vascular function in acute myocardial infarction, and is unable to recognize the early vulnerable plaque.

Computational fluid dynamics (CFD) has been widely used for analyzing the hemodynamic significance in abnormal vasculatures [14], [15]. FFR computed from CFD analysis based on the reconstruction from CTA images has been developed to assist in the diagnosis of coronary artery stenosis [16]. However, the accuracy of the current FFRCT algorithm is still suboptimal, as the reconstruction of arterial geometries from CTA is associated with distribution of the contrast agent and the blurring effect in the edges. Therefore, the accuracy of the reconstructed vascular geometries from CTA images is limited and so as the FFR calculated from the according geometries [17]–[21]. Recent studies have applied CFD to the computational of virtual FFR [22]–[24]. It could obtain good accuracy, but it needs many hours to calculate, and so the method still needs to be improved.

Therefore, it is important to combine IVUS with CAG to evaluate the FFR value of a stenotic coronary artery. Based on computed FFR value and IVUS examination, the optimal treatment strategy can be selected for the patient. CAG shows all the information of coronary artery tree to evaluate coronary artery stenosis, including coronary origin and its anatomical variation. IVUS can be used for clinical evaluation, such as the severity of coronary artery stenosis, the lesion length and plaque feature of coronary artery plaque; it may also be possible to further miniaturize the catheter.

In order to overcome the limitations of these previous methods, we have adopted a method, combining the CAG images with the IVUS images to reconstruct the three-dimensional coronary vascular model, and to more accurately obtain a measure of the stenosis severity and the geometric characteristics of the coronary lesion based on coronary hemodynamics analysis. We have noted that TIMI (Thrombolysis In Myocardial Infarction) frame count [25], [26] can be employed to calculate the mean volumetric flow rate through the boundaries of reconstructed coronary artery vessel with hyperemic projections. By combining this information with hemodynamic CFD analysis, pressure across the coronary stenosis were calculated to determine the values of flow based FFR (fFFR). Then the evaluation of correlation and agreement between calculated fFFR and the measured FFR (mFFR) obtained by using pressure-guided wire invasive approach was preformed. Additionally, the correlations between fFFR and the geometric characteristics of the coronary lesions (the severity of the stenosis, the curvature of the lesion, the length of the lesion, the tortuosity of the lesion and the angle of the immediate downstream of the lesion) are also assessed, in order to provide a comprehensive understanding of the coronary hemodynamics and related diagnostic information. This has also helped to evaluate the accuracy of the reconstructed coronary artery vascular structure.

This paper is organized as follows. In Section II, Material and Methodology is discussed, which includes Study Population and Measurement of Pressure wire-derived FFR, 3-D reconstruction of coronary arteries, CFD simulation, and determination of the coronary lesion parameters. Section III includes the experimental results of 3-D Catheter Trajectory Reconstruction, 3-D Reconstruction of Coronary Artery, CFD simulation, and correlation of the coronary lesion geometric parameters with fFFR. Then, Discussion and Conclusion are elucidated in sections IV and IV.

II. MATERIAL AND METHODOLOGY

In this paper, we propose a method, to combine the CAG images within spatial geometrical information with the IVUS images within the cross-sectional information, to reconstruct the three-dimensional vascular model and to obtain the stenosis and geometric characteristics for CFD based hemodynamics analysis to compute Fractional Flow Reserve (FFR) according to the work-flow shown in Fig.1

The CAG and IVUS images are obtained by means of the Angiographic and Intravascular Ultrasound apparatus. Initially, when preprocessing the CAG images, the catheter 2D curves are segmented based on the eigenvalues of Hessian matrix [25], to estimate the catheter trajectory curve in the 2-D angiographic image. The reconstruction of 3-D catheter trajectory is obtained by the vertical intersection of two curved surfaces, generated by the 2-D catheter curves extracted vertically to their angiographic planes and intersected with each other. The vascular edges are detected by

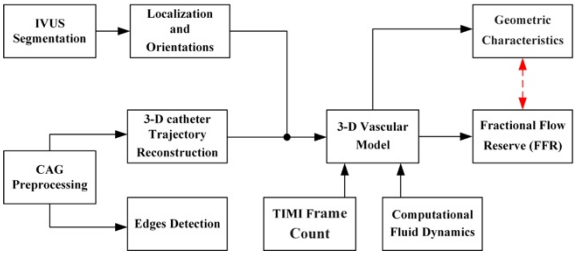

FIGURE 1. Work-flow of this study for 3-D reconstruction.

the Gaussian and Laplacian filter (LoG), for the subsequent determination of the spatial orientation of the IVUS images.

The acquired IVUS images are loaded into the IVUS Angio tool [28] (a publicly available software for endovascular image processing, Thessaloniki, Greece, http://mklab.iti.gr/ivus). The end-diastolic IVUS images are automatically selected using Electrocardiograph (ECG), and the IVUS contours are segmented by a semi-automatic method. According to the acquisition order and spacing of the IVUS images, the inner and outer vascular contours (i.e. the IVUS images) are placed vertically in order along the reconstructed 3-D IVUS catheter trajectory to determine the localization of each image, and the relative orientation of each image is calculated by establishing the Frenet-Serret formula [29], [30] in the reconstructed 3D catheter path. The whole set of IVUS images is rotated by 5 degrees for each rotation up to 360 degrees, and back-projected to the two angiogram planes, in order to calculate the minimum error distance compared to the vascular edges in the angiogram planes. Then, the determination of the relative and absolute orientation of the IVUS images is carried out, and fusion of IVUS and CAG is completed to obtain the 3-D vascular model.

Then the Geometric characteristics are calculated from the reconstructed 3-D vascular models for geometric analysis. The vascular model is subjected to grid partitioning to generate a grid model, and then the transit time of contrast agent is calculated by using the TIMI frame count with hyperemic projections in the boundaries of the reconstructed coronary artery vessel. The mean volumetric flow rate at hyperemia state is equal to the lumen volume of the reconstructed model divided by the mean transit time. Then, the relationship between the mean pressures at the inlet and outlet and the flow rate can be obtained by means of the Navier-Stokes equations. The values of the fFFR are calculated from the mean pressures at the outlet and at the inlet. The correlations between the values of fFFR and the geometric characteristics of coronary artery are evaluated in this work, as shown in red double arrow part of Fig.1. This method makes full use of the advantages of IVUS examination to evaluate FFR and diagnose the severity of the disease. It eliminates the introduction of the pressure wire based invasive FFR measurement, and could thereby reduce the risk of perforation and splitting of the coronary plaque.

A. STUDY POPULATION AND OBTAINING CAG IMAGES AND IVUS IMAGES

Study Population. 20 patients with 22 coronary arteries (including 3 right coronary arteries [RCA], 1 left main coronary artery [LM], 1 left circumflex [LCx], 17 left anterior descending arteries [LAD]) in total were included in this work. They were diagnosed with cardiovascular disease such as stable or unstable angina or stenosis, and the average age ranged from 48 to 72 years old. The data of this study was obtained with the written informed consent forms from all of the patients. The selection criteria were including, but not limited to, patients able to receive adenosine or iodine-based contrast media and invasive coronary angiography; Intravascular Ultrasound (IVUS), and FFR assessment with recorded hyperemic projections were implemented, and the image quality of the hyperemic projection was adequately evaluated by frame count.

Obtaining CAG Images and IVUS Images. During the process of obtaining images, the angiography catheter was inserted into the ostium of the left or right coronary arteries by percutaneous puncture into the thigh femoral artery. The 0.014 inch guidewire, which includes the IVUS catheter with a miniaturized ultrasound probe at the tip, was inserted into the distal end of coronary artery (i.e., the starting point of IVUS catheter withdrawal) through the angiography catheter. The contrast agent was injected into coronary arteries by the angiography catheter to visualize the IVUS catheter and the edge of the vascular lumen, and to record coronary angiography (CAG) images. Thereafter, under the guidance of the X-ray images, the IVUS catheter was automatically withdrawn to record IVUS images from the distal end of coronary artery to the exit of the angiography catheter at a constant speed. The acquisition of CAG images and IVUS images were completed. Then, the angiography catheter and the guidewire were removed from the patients. All the recorded images were stored in the DICOM (Digital Imaging and Communications in Medicine) format. Moderate amounts of nitroglycerin was injected to fully expand the coronary arteries to exclude spasm before the coronary angiography. Electrocardiograph (ECG) was used to acquire IVUS images at the same cardiac phase, which reduced influence of periodic movements of the heart and respiration.

B. 3-D RECONSTRUCTION OF CORONARY ARTERIES

CAG Preprocessing. Coronary (X-ray) Angiography (CAG) was carried out by puncturing the special catheter from the thigh femoral artery or radial artery of upper limb into the coronary ostium under local anesthesia. Special X-rays were taken to record the coronary angiogram, while the contrast agent was flowing through coronary arteries. Due to disturbance by various factors while obtaining CAG images, this may generate much noise, like Gaussian noise, salt, and pepper noise. So firstly, image enhancement was implemented to improve the image quality and to remove some artifacts, such as similar to the blood vessels of bones and muscle tissue.

Then next, the Gaussian low-pass filter was used as an image smoothing operation [31].

IVUS Segmentation. IVUS acquisition was carried out by sending the IVUS catheter into the distal end of the coronary artery. The IVUS catheter was retreated at a constant speed, so the IVUS images were considered to be equally distributed along the catheter, and each plane (which included the IVUS images) could be deemed to be perpendicular to the tangent vector of the catheter at the corresponding point [32]–[34]. All of the acquired IVUS images were imported into the IVUS Angio tool to segment the lumen and media-adventitia border, by combining with ECG or selected end-diastolic images manually at the same time [27]. A point cloud in a text file was exported and continued for further processing.

Edges Detection of CAG images. Edges detection of CAG images was realized by using serial application of the Laplacian filter and the Gaussian filter, with computation of the second derivative of the CAG images by the Laplacian operator∇^2, and the use of the Gaussian filter to smoothen the images and emphasize the gray information of the blood vessel.

3-D Catheter Trajectory Reconstruction. The 3-D catheter trajectory reconstruction is shown in Fig.2A. Firstly, the eigenvalue and eigenvector of the Hessian matrix were used to estimate the catheter trajectory curve in the 2-D angiographic image. A satisfactory vascular catheter curve can be obtained by interpolating and final fitting. According to the mathematical theory, then the 3-D spatial curve can be derived from the intersection of two surfaces. The starting point for catheter withdrawal was fixed from the clinical imaging of CAG and IVUS. The extracted 2-D catheter curves could be moved to the same height (the same Z coordinates in the same coordinate system), and then extracted perpendicularly and intersected with each other to generate the 3-D catheter trajectory during the reconstruction procedure. For calculating the discrete points to obtain the 3-D catheter trajectory from the actual computation of surfaces intersection, the method of setting the threshold value was used. When the difference between the Z coordinates of the two surfaces at the same grid point was smaller than the specified threshold, the grid point was no doubt recognized as the intersection. Nevertheless, the threshold value needed to be set several times in order to achieve the ideal precision.

Localization and Orientations of IVUS Frames. According to the acquisition order and the spacing of the IVUS images, the inner and outer vascular contours are placed in order by the rotation transformation and the translation transformation along the reconstructed 3-D IVUS catheter trajectory, to determine the localization of each image as shown in Fig.2B. Then, the determination of the angle of the entire set of IVUS images is carried out in the following two steps: the relative orientation between consecutive frames of the IVUS images, followed by the absolute orientation of the whole set of IVUS image sequences.

The relative orientation between consecutive frames of the IVUS images [29], [30], [34]: The IVUS catheter was always bent when inserted into the blood vessel, and so it was treated as a 3-D spatial curve, involving curvature and twist, which could be calculated by using the Frenet-Serret formula. We designated the angle of the first IVUS frame manually, and then determined the relative angle of each later frame compared to the first frame, after which the relative orientations of the entire set of IVUS frames was calculated.

The absolute orientation of the IVUS images: The absolute angle of the entire set of IVUS images was computed as a rigid body model. The whole set of IVUS images was rotated by 5 degrees for each rotation up to 360 degrees, and back-projected to the two angiogram planes to calculate the error distance compared to the actual vessel lumen. The derived angle would then be the best absolute angle of IVUS image

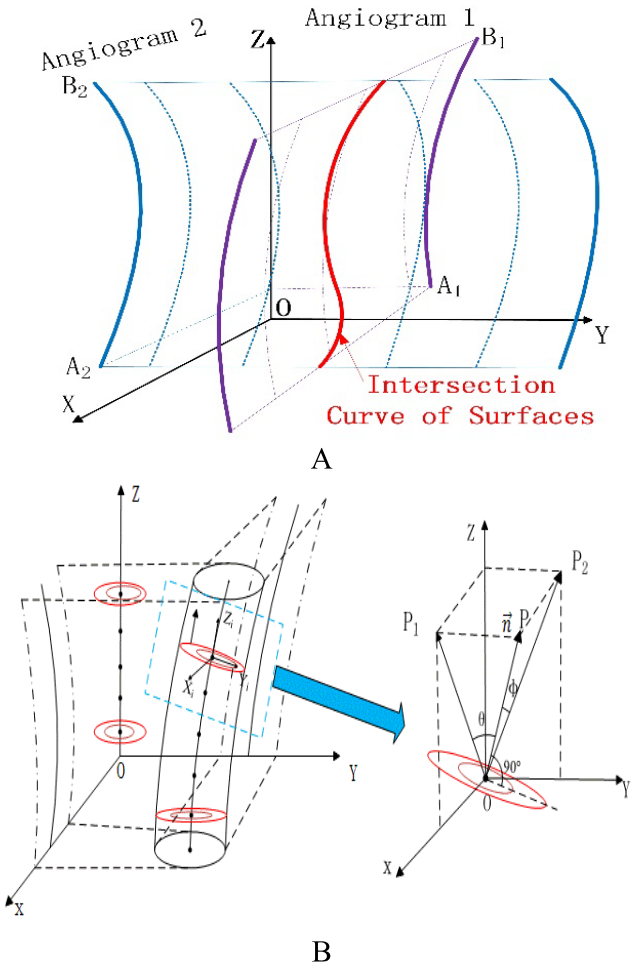

FIGURE 2. Figure 2A is the schematic diagram of 3-D catheter trajectory reconstruction, where A_1 and A_2 represent the starting points for acquiring the CAG and IVUS images, and B_1 and B_2 are the end points. The 3-D catheter trajectory is obtained by vertical extraction and intersection. Figure 2B is a schematic drawing that illustrates the localization of IVUS frames and the rotation mode. The IVUS plane is perpendicular to the catheter when the angle between the normal vector $\vec{n}$ of the IVUS plane and the tangent vector corresponding point on the catheter is zero, in which $\overrightarrow{OP}$ is $\vec{n}$, P_1 and P_2 are P projects to the XOZ plane and YOZ plane and θ and φ the angle between $\vec{n}$ and $\overrightarrow{OP_1}$ and $\vec{n}$ and $\overrightarrow{OP_2}$.

sequences while the distance was obtained as the minimum cumulative sum.

C. CFD SIMULATION OF HEMODYNAMICS ANALYSIS

The hemodynamic parameters, such as the features of the blood vessels and blood were simulated to evaluate the fFFR values from the newly obtained 3-D vascular model. This research is concentrated on the peak flow velocity stage of hemodynamics in the coronary artery, for which the flow distribution is assumed to be fully developed. For this purpose, we have assumed that the coronary artery vessels are impermeable, and the walls of the vessels are rigid with no slip boundaries. The blood was assumed to be Newtonian and incompressible, while the blood flow for simulation was assumed to be unsteady flow and adiabatic laminar flow. Appropriate values of the blood rheological parameters were applied for the blood viscosity coefficient of 0.0035 Pa · s and blood density of 1056 kg/m3 [35], [36].

The transit time of the contrast agent was calculated by using the TIMI frame count for hyperemic projections of the reconstructed coronary artery vessel. The shortest transit time was used from the available multiple hyperemic projections. The mean volumetric flow rate in the hyperemia state was computed to be equal to the lumen volume of the reconstructed coronary artery divided by the mean transit time. The mean hyperemic volumetric flow rate and the mean pressure at the guiding catheter tip were applied at the inlet, whereas the fully developed flow (out flow) condition was applied at the outlet. The reconstructed geometries were then discretized with tetrahedral cells (meshing). Then, the mass conservation and flow momentum of blood flow were solved in each cell, according to the Navier-Stokes equations [37], [38]:

$$(\nabla \cdot \mathrm{u}) = 0 \tag{1}$$

$$\rho\left(\frac{dV}{dt} + \mathrm{u} \cdot \nabla \mathrm{u}\right) = -\nabla P + \mu \nabla^2 u \tag{2}$$

where P is the pressure, u is the velocity field, ρ and μ are the density and viscosity coefficient of the blood fluid, respectively. The output data of pressures at the outlet and inlet were computed from the input data, which were the assumed vascular parameters and the mean volumetric flow rate at hyperemia after simulation in the N-S equation. Then, fFFR was defined as the mean pressure at the outlet divided by the mean pressure at the inlet. Based on the above equations, the simulation process was performed in COMSOL Multiphysics (COMSOL AB, Stockholm, Sweden) and multifrontal massively parallel sparse direct solver (MUMPS) [39].

D. DETERMINATION OF THE CORONARY LESION GEOMETRIC PARAMETERS

The parameters of tortuosity of the lesion segment, the curvature of the lesion, the angle of the direct downstream lesion, the length of the lesion, the severity of the stenosis and such geometrical parameters for the vascular model were obtained from the three-dimensional coronary artery reconstruction based on CAG and IVUS, as described above. The ratio of the length from the ostium of the coronary segment to the distal 1 cm of the stenosis to the distance between the ends of the segment was called the tortuosity of the lesion segment. The curvature (unit: 1/m) of the stenotic arteries was measured at the peak stenosis. The angle (unit: degree) of the lesion was measured at the immediate distal margin of the vessel lesion. The length (in mm) of the stenosis was measured at both ends of the stenosis. The ratio of the cross-sectional area of the vessel lumen at the stenosis and the cross-sectional area of normal vascular lumen at the adjacent segment was considered as the measure of severity of the stenosis.

E. MEASUREMENT OF PRESSURE WIRE-DERIVED FFR

Fractional flow reserve (FFR) measurement, based on the relationship between coronary artery pressure and blood flow, is the gold standard in the functional assessment of the coronary blood perfusion. FFR is thus defined as the ratio between the maximum achievable blood flow in the diseased coronary artery and the theoretical maximum flow in a normal coronary artery, and is determined by the ratio of pressures across the stenosis during maximal coronary hyperemia. FFR (mFFR) is measured during cardiac catheterization by using a pressure-temperature sensor guidewire that is placed across the significant stenotic lesion. The pressure measurement starts from a position downstream of the lesion. The maximal hyperemia was induced by using a vasodilating agent, such as intravenous or intra-arterial adenosine (140 μg/kg/min). The proximal arterial pressure (Pa) and distal arterial pressure (Pd) were measured, and FFR was calculated by dividing the mean distal coronary pressure (mPd) by the mean aortic pressure (mPa) during hyperemia. The FFR data along the pressure wire were performed as the gold standard for the assessment of our methodology based on the fusion of IVUS and X-ray angiography-based FFR estimations.

III. RESULTS

A. CORRELATION OF THE RECONSTRUCTED 3-D CATHETER

Trajectory with that of the original 2D Catheter in the Angiographic PlanesWe now compare the results of correlation of the reconstructed 3-D catheter trajectory back-projected to the XOZ (RAO), YOZ (LAO) plane with the angiographic planes of the 2-D catheter guide wire, as shown in Figs.3 and.4. We set the Y/Z coordinates of the 2D catheter in the angiographic plane (YOZ plane) as ''The original Y/Z coordinates of angiography'', and the X/Z coordinates of the 2D catheter in the angiographic plane (XOZ plane) as ''The original X/Z coordinates of angiography'' in the coordinate system. The X/Y/Z coordinates of the reconstructed 3-D catheter trajectory back-projected to the two angiographic planes were set as ''The X/Y/Z coordinates of the 3D catheter trajectory'' in the coordinate system. The charts show the units of the values in millimeters (mm). Obviously, relevance

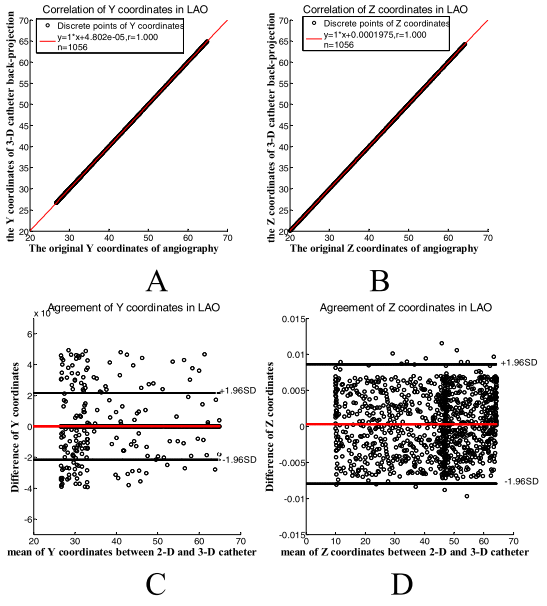

FIGURE 3. Figures 3A and 3B show the correlation of Y and Z coordinates between 3-D catheter trajectory back-projected to the YOZ plane and the 2-D catheter. Figures 3C and 3D depict the agreement between them. The correlation of Y ($y = 1 * x + 4.802e - 05$, $r = 1.000$, $P < 0.001$) and Z ($y = 1 * x + 0.0001975$, $r = 1.000$, $P < 0.001$) coordinates are between the 3-D catheter trajectory back-projected to the YOZ plane and the coordinates of 2-D catheter. The agreement of the Y coordinates between the 3-D catheter trajectory and the coordinates of 2-D catheters is $2.4923e - 05 \pm 1.96 * 0.0011$ mm. The agreement of the Z coordinates is $3.6039e - 04 \pm 1.96 * 0.0042$ mm.

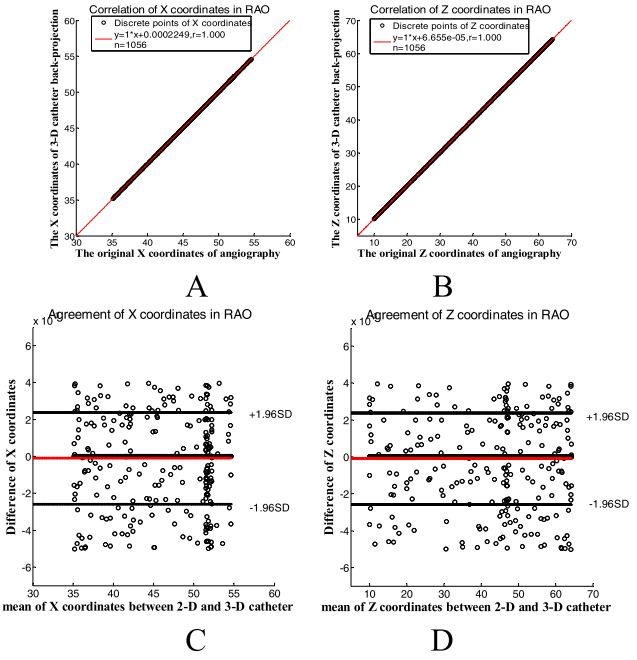

FIGURE 4. Figures 4A and 4B show the correlation of X and Z coordinates between 3-D catheter trajectory back-projected to the XOZ plane and the 2-D catheter. Figures 4C and 4D depict the agreement between them. The correlation of X ($y = 1 * x + 0.0002249$, $r = 1.000$, $P < 0.001$) and Z ($y = 1 * x + 6.655e - 05$, $r = 1.000$, $P < 0.001$) coordinates are between the 3-D catheter trajectory back-projected to the XOZ plane and the coordinates of 2-D catheter. The agreement of the Z coordinates and X coordinates are $-9.0182e - 05 \pm 1.96 * 0.0013$ mm.

is noted to be particularly high between the 3-D trajectory and the 2-D catheter guide wires. The correlation of Y ($y = 1 * x + 4.802e - 05$, $r = 1.000$, $P < 0.001$, $n = 1056$) and Z ($y = 1 * x + 0.0001975$, $r = 1.000$, $P < 0.001$, $n = 1056$) coordinates between the 3-D catheter trajectory back-projected to the YOZ plane and the 2-D catheter are pretty high, after simple linear programming as shown inFigs.3A/3B, wherein the horizontal coordinates denote the Y coordinate and Z coordinate of the 2-D catheter in the YOZ (LAO) plane respectively, and the vertical coordinates indicate the Y coordinate and Z coordinate of the 3-D catheter curve back-projected to the YOZ plane. Due to a wide range of curvilinear coordinate values caused by the larger number of points ($n = 1056$), the fitting curves are almost coincident with $y = x$, while the differences are relatively small. Similarly, for the same coordinate parameters setting in Fig.4A/4B, the corresponding analysis and regression equations for X and Z in RAO are $y = 1 * x + 0.0002249$ and $y = 1 * x + 6.655e - 05$, respectively ($r = 1.000$, $P < 0.001$, $n = 1056$).

The Bland-Altman graphs show the agreement of the 3-D catheter trajectory and the 2-D catheter in Figs.3C/3D and 4C/4D. The horizontal coordinates of Figs 3C/3D are the Y/Z coordinates corresponding to the average of the difference between the 2-D guide wire and 3-D catheter back-projected to the YOZ (LAO) plane; the vertical coordinates are the bias of the difference. It is similar in Fig.4C/4D. The mean value of the difference and the standard deviation of X coordinates in the RAO plane are −9.0182e-05 mm and 0.0013 mm, and similarly for the Z coordinates. For the Y coordinates in the LAO, we have 2.4923e-05 mm and 0.0011 mm, and for the Z coordinates 3.6039e-04 mm and 0.0042 mm.

Only the differences of less than 100 points are outside the ±2SD when calculating more than 1000 points. For the Z coordinates of the catheter in the LAO plane used as a reference to calculate the 3-D trajectory, most of the differences are in the ±2SD compared to the other coordinates.

B. RESULTS OF THE PROCESS OF 3-D RECONSTRUCTION OF CORONARY ARTERY

Fig 5 shows the results of our 3-D Coronary Artery reconstruction process, involving the segmentation of the IVUS contours, the 3-D catheter trajectory reconstruction through CAG, fusion of IVUS images and catheter, localization and orientations of IVUS Frames. All these works were accomplished in the Matlab. Figure 5A is segmented for getting the inner and outer contours by IVUS Angio tool software, and it is loaded into Matlab to process and draw. The red lines in Figure 5B is the 3-D catheter, obtained from the resultant 2D curves extracted vertically to their angiographic planes and intersected with each other. The blue lines are the vascular contours and 2-D catheter in the XOZ plane. The pink lines are the vascular contours and 2-D catheter in the YOZ plane.

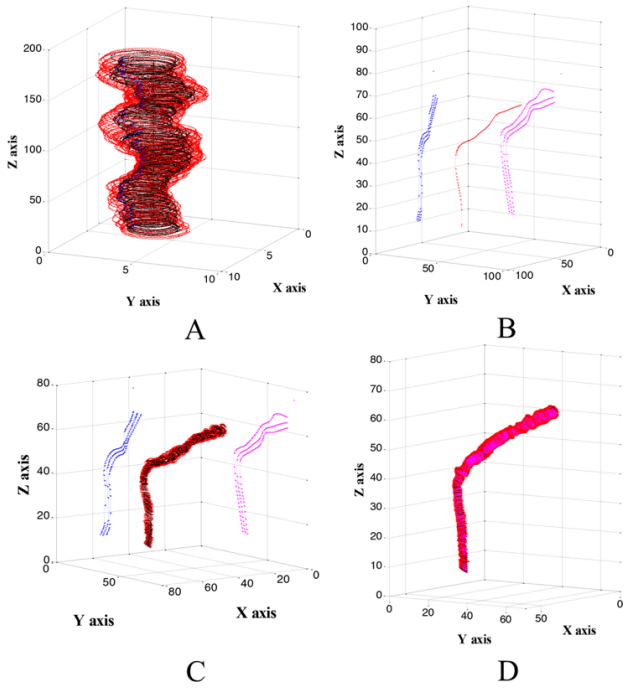

FIGURE 5. The results of the 3-D reconstruction method of our work. Figure 5A is segmented for getting the inner and outer contours by the IVUS Angio tool software, and it is then loaded into MATLAB for processing and drawing. The red lines in Figure 5B is the reconstructed 3-D catheter, obtained from the resultant 2D curves extracted vertically to their angiographic planes and intersected with each other. Figure 5C shows the localization and orientations of IVUS Frames in the reconstructed 3-D catheter. Figure 5D shows the final three-dimensional construction results of the 3-D vascular mode.

Figure 5C is the fusion of the inner and outer vascular contours and the 3-D catheter by the localization and orientations of the previous analysis. Figure 5D shows the final 3-D vascular model.

C. CFD DERIVED fFFR CALCULATION VALIDATION

The CFD validation is performed by comparing the CFD derived fFFR and the mFFR value, as shown in Fig.6. Therein, Fig.6A shows the Bland-Altman agreement test between the mFFR and fFFR, with mean $\pm 1.96 * \text{SD}$ being -0.0094 ± 0.0932. Fig .6B shows the good correlation between the calculations and measurements ($r = 0.916$, $y = 0.8539 * x + 0.1223$).

Another important correlation coefficient, the Spearman correlation coefficient, was calculated to be equal to 0.919; this indicates that these two values have good agreement.

D. CORRELATION OF THE CORONARY LESION GEOMETRIC PARAMETERS WITH THE fFFR VALUES

The effects of the geometric characteristics of the coronary lesion on the coronary artery pressure distribution and the maximum WSS at the stenosis are now presented in Fig 7. These coronary lesion geometric characteristics include the severity of the stenosis, the curvature of the lesion, the tortuosity of the lesion, the length of the lesion, and the angle

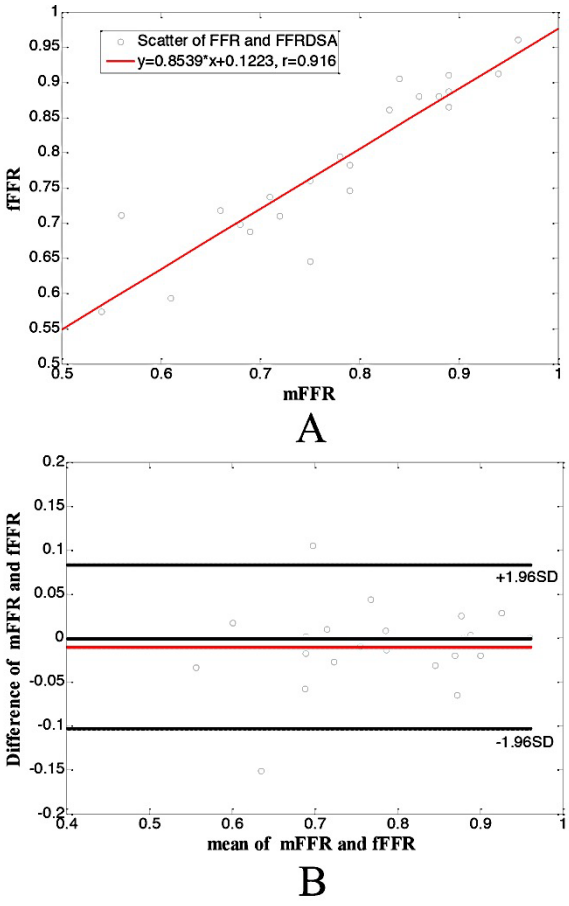

FIGURE 6. Validation of the CFD derived calculation of fFFR is provided by comparing the calculated fFFR to mFFR. A: Agreement between the fFFR and FFR is evaluated by Bland-Altman agreement test, with mean $\pm 1.96 * \text{SD}$, bias of -0.0094 ± 0.0932. B: Agreement between fFFR and FFR is also evaluated by linear regression: $r = 0.916$, $y = 0.8539 * x + 0.1223$.

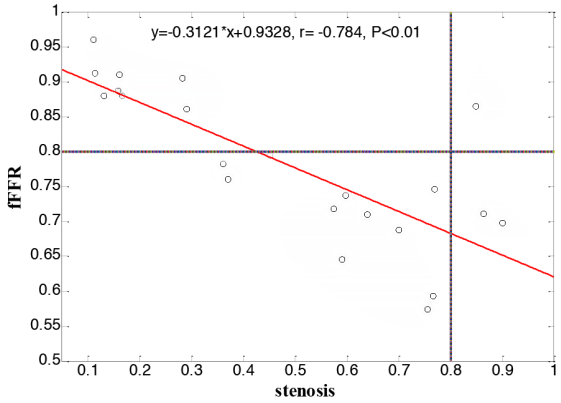

FIGURE 7. The correlation analysis of fFFR and the Severity of the stenosis. The correlation factor r was -0.784 with $y = -0.3121 * x + 0.9328$. The two color lines are fFFR of 0.8 and the severity of the stenosis of 0.8. Obviously, it shows a negative correlation. The fFFR value was getting lower with the increase in the severity of the stenosis.

of the immediate downstream of the lesion. The correlation between fFFR and the severity of the stenosis was found to be significant as shown in Fig.7, where the two color lines are

fFFR of 0.8 and the severity of the stenosis of 0.8. Obviously, it shows a negative correlation ($y = -0.3121 * x + 0.9328$, $r = -0.784$) between fFFR and the severity of the stenosis. The fFFR value is seen to be getting lower with the increase in the severity of the stenosis.

The fFFR distribution in coronary arteries with stenosis is shown in Fig.8. It can be seen that when the severity of stenosis increased, the fFFR values decreased at the stenosis. The degree of the stenosis in A, B and C is shown to be 11.23%, 16.57% and 28.21%; the corresponding fFFR values are 0.912, 0.88 and 0.905, respectively. The degree of the stenosis in D, E and F was 37.07%, 57.39% and 59.7%; the corresponding fFFR values were 0.76, 0.7177 and 0.737, respectively. The degree of the stenosis in G, H and I was 76.64%, 75.59% and 86.36%; the corresponding fFFR values were 0.593, 0.574 and 0.711, respectively.

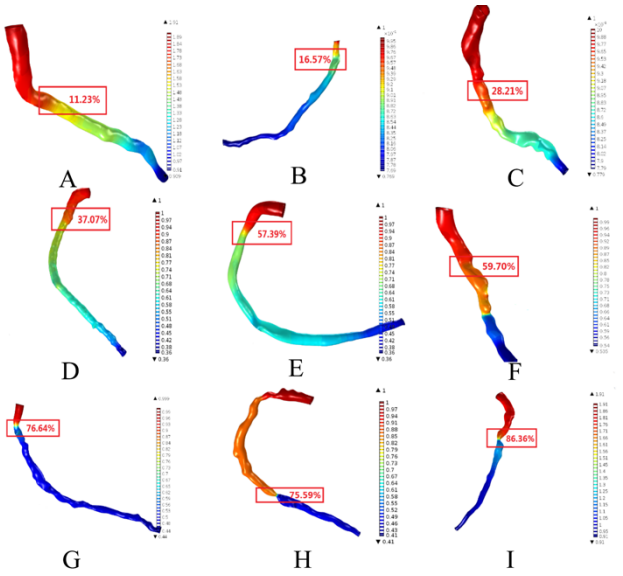

FIGURE 8. The fFFR distribution in the coronary arterial geometries with stenosis. The fFFR at the stenosis decreased as the severity of the stenosis increased, as shown in Figures 8A-8I. . The degree of stenosis in A, B and C was 11.23%, 16.57% and 28.21%; the corresponding fFFR values were 0.912, 0.88 and 0.905, respectively. The degree of stenosis in D, E and F was 37.07%, 57.39% and 59.7%; the corresponding fFFR values were 0.76, 0.7177 and 0.737, respectively. The degree of stenosis in G, H and I was 76.64%, 75.59% and 86.36%; the corresponding fFFR values were 0.593, 0.574 and 0.711, respectively.

The relationship between fFFR and the maximum WSS at the stenosis, and the relationship between the maximum WSS and the severity of stenosis at the lesion are presented in Fig.9. The value of fFFR decreased with the increase of the maximum WSS, according to the relationship of the fFFR and the maximum WSS shown in Fig.9A ($r = -0.723$, $P < 0.01$). Fig.9B shows the maximum WSS at the lesion growth to be in direct proportion to the severity of stenosis ($r = 0.614$, $p < 0.01$). This means that the severity of stenosis increase would lead to the decreased value of fFFR, the same as depicted in Fig.7.

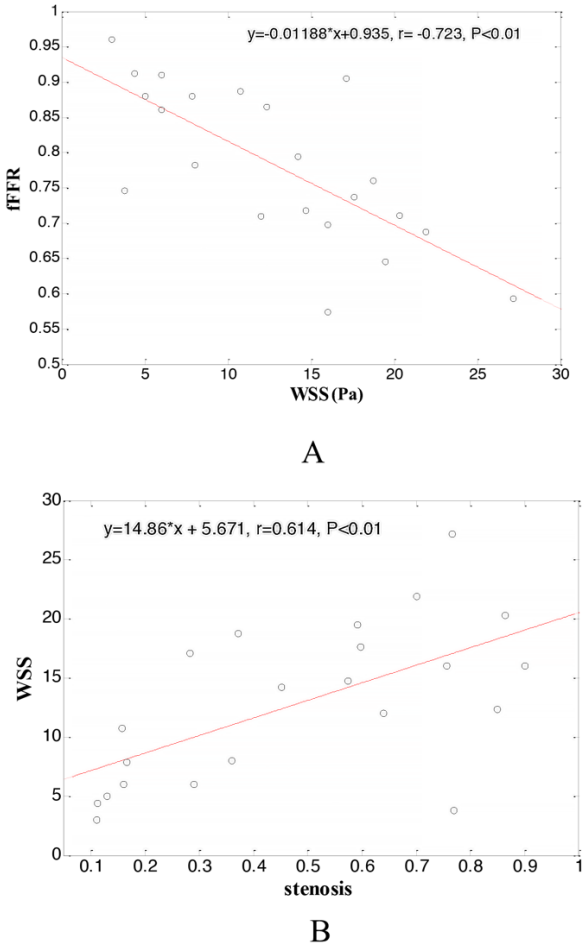

FIGURE 9. The fFFR distribution in the coronary arterial geometries with the maximum WSS at the lesion. The fFFR at the lesion decreased as the WSS increased, as shown in the figure. A: The Pearson correlation between fFFR and WSS was found to be significant ($r = -0.723$, $y = -0.01188 * x + 0.935$, $P < 0.01$). The Spearman correlation between fFFR and WSS was found to be significant and equal to −0.708. B: The correlation between the severity of the stenosis and WSS was also found to be significant ($r = 0.614$, $P < 0.01$).

However, the fFFR value was found to have no significant correlations to the curvature of lesion ($r = -0.342$, $P = 0.119$), the tortuosity of the lesion segment ($r = -0.278$, $P = 0.210$), the lesion length ($r = -0.216$, $P = 0.335$), and the angle of the direct downstream of the lesion angle ($r = 0.278$, $P = 0.210$), as shown in Fig.10.

IV. DISCUSSION

A. EVALUATION OF 3-D CATHETER RECONSTRUCTION

Three-dimensional reconstruction of the coronary artery from fusion of IVUS and CAG images combined lumen geometry and arterial route had enable accurate evaluation of the anatomic characteristic of the coronary artery and clinical implementations. Prasad et al. demonstrated that geometries reconstructed from co-registration of IVUS and angiography resulted in mean error of 0.35mm compared to the angiography [40]. Compared to the present study, evaluation the

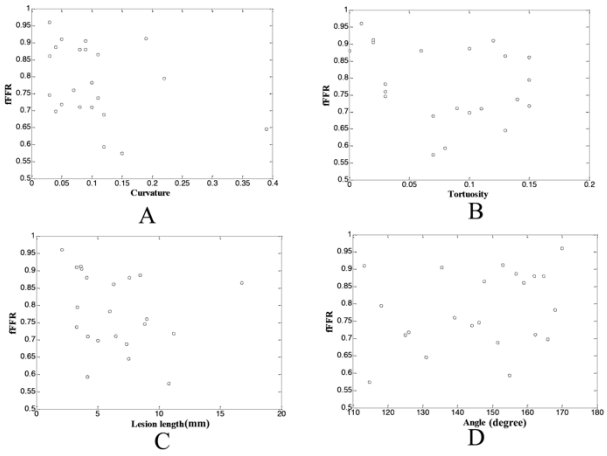

FIGURE 10. Relationship of fFFR with stenosis severity, tortuosity, curvature, angle, lesion length in the reconstructed patient-specific coronary arteries. A: effect of curvature on fFFR; B: effect of tortuosity on fFFR; C: effect of lesion length on fFFR; D: effect of angle of the lesion segment on fFFR. All of these vascular structural parameters were not significantly associated with fFFR.

reconstructed geometry was performed by back-projected to the corresponding 2-D coronary angiography plane as showed in Figs 3 and 4. By back-projecting to YOZ plane, high correlations of the Y-coordinate ($y = 1*x+4.802e-05$, $r = 1.000$, $P < 0.001$) and Z-coordinate ($y = 1 * x + 0.0001975$, $r = 1.000$, $P < 0.001$) was found and the good agreements of Y-coordinate (0.025 ± 0.011mm) and Z-coordinate (0.036 ± 0.042mm) were obtained.

It can be suggested that the 3-D catheter reconstruction was well performed according to the method presented in this paper, which will lay a good foundation for the establishment of the subsequent coronary vascular stenosis models. Compared with the other methods of establishing the coronary vessel model [31], [41], this method makes full utilization of the spatial information of the CAG images and the cross-sectional information of IVUS images to accurately compute the 3-D vascular model, so as to provide a good prerequisite for subsequent hemodynamic simulation.

B. EVALUATION OF CFD SIMULATION OF HEMODYNAMIC ANALYSIS FOR CALCULATION OF fFFR

Based on the fusion of CAG and IVUS images, we have developed a new computerised coronary vascular model to quickly calculate FFR (fFFR). The three-dimensional vascular model was subjected to grid partitioning to generate a grid model for numerical simulation of blood flow. The hemodynamics study was concentrated in the peak flow velocity stage, and the flow distribution was assumed to be fully developed. The transit time of contrast agent was calculated by using the TIMI frame count on hyperemic projections, and the mean volumetric flow rate at hyperemia was obtained from the reconstructed coronary lumen volume and the transit time.

The relationship between the mean hyperemic volumetric flow rate and the unknown mean pressures was calculated from the application of the Navier-Stokes equations at the inlet and outlets to the coronary stenosis. Then the fFFR value was defined as the mean pressure at the outlet divided by the mean pressure at the inlet. We then analyzed the relationship between the calculated fFFR by fusion with IVUS and CAG, and the pressure wire measured mFFR values. It had a good correlation ($r = 0.916$, $P < 0.01$) and agreement ($\text{mean} + 1.96 * \text{SD} : -0.0094 \pm 0.0932$), as shown in Fig 6.

Compared to accessing mFFR values by inserting a catheter using a sheath and pressure guide wire [42], fFFR was obtained through the use of CFD hemodynamic analysis based on the fusion of IVUS and CAG. While patients were asked to do IVUS examination and invasive FFR after the doctor's primary diagnosis, this method made full use of the advantages of IVUS and CAG examination to evaluate the fFFR. The validation of the calculated fFFR method can serve to eliminate the introduction of the pressure wire. Meanwhile, our method also took full advantage of IVUS to diagnose the diseases which FFR cannot recognize, and to guide the interventional treatment program. Hence, it can reduce the patient risk as well as enable more elaborate computation of FFR along with the geometric features of the coronary lesions. Further, our method for calculating the pressures at the outlet and inlet of the coronary lesion, by means of CFD hemodynamic analysis in the reconstruction coronary vascular model, is more flexible and more efficient, and can enable more patients with coronary artery stenosis to be reliably diagnosed and treated in equal time.

C. EVALUATION OF THE EFFECT OF THE CORONARY LESION's GEOMETRIC CHARACTERISTICS ON fFFR

We have analyzed the correlation between fFFR and the geometric characteristics of the coronary lesion, namely the severity of stenosis coronary artery, the maximum WSS at the lesion, the curvature of lesion, the tortuosity of the lesion segment, the lesion length and the angle of the direct downstream of the lesion. The different fFFR values corresponding to the coronary artery model with different degrees of stenosis were demonstrated in Fig.8. The relationship between fFFR and the severity of stenosis was obtained from Fig.7 ($r = -0.784$, $P < 0.01$). The more severe the stenosis, the lower the fFFR value, and greater the likelihood of myocardial ischemia [13]. Also, the maximum WSS at the lesion was positively correlated with the degree of stenosis ($r = 0.614$, $P < 0.01$), and negatively correlated with the fFFR values ($r = -0.723$, $P < 0.01$). These correlations of lesion parameters with fFFR can have a significant impact on the diagnosis as well as the treatment of coronary artery stenosis by percutaneous coronary intervention (PCI) as to whether a stent needs to be placed in the stenosis

The curvature of lesion, the tortuosity of the lesion segment, the lesion length and the angle of the direct downstream of the lesion were not significantly correlated with the fFFR values. However, these geometric features of the lesion can

have influence on the analysis of flow characteristics and flow parameters. For instance, the curvature of lesion and the lesion length may affect blood flow velocity and maximum WSS resulted in of the fFFR values [43], [44]. Previous study showed that joint effect of the curvature and the angle of the stenotic vessel was significant correlated with maximum flow velocity through the stenosis [45]. Therefore, instead of separate characteristic, the combination of various geometric characteristics of the coronary artery have complex influence on the hemodynamic redistribution in the diseased coronary arteries.

D. CLINICAL VALUES OF fFFR

FFR had been developed for functional assessment of coronary arterial stenosis. IVUS can be used for clinical evaluation, such as the severity of coronary artery stenosis, the lesion length and plaque feature of coronary artery plaque. Despite of the catheterization requirement for both CAG and IVUS, IVUS was better in diagnosing more extensive types of coronary lesions, and guiding percutaneous coronary intervention therapy in combination of FFR measurement. However, the additional catheterization and radiation from the invasive procedures resulted in adverse reactions from patients, which limited the application of multiple modalities in clinical decision-making.

Therefore, the approach we have adopted in this study has made full use of the advantages of IVUS and CAG examination to evaluate the fFFR, so as to assess the vascular function and to characterize the severity of coronary lesions. It can eliminate the introduction of the pressure wire and mitigate these adverse effects of using a pressure guide wire to measure FFR values. Meanwhile, it has taken full advantages of IVUS to assess vascular function in acute myocardial infarction and to diagnose the lesions (e.g. vulnerable plaque), which FFR cannot recognize, and to guide the interventional treatment program. Our method for calculating the fFFR values, by means of CFD hemodynamic analysis in the reconstruction coronary vascular model, is more flexible and more efficient, and can enable more patients with coronary artery stenosis to be reliably diagnosed and treated in equal time. It can thereby provide a good measure of monitoring and guiding the coronary treatment program [46]–[48].

E. STUDY LIMITATIONS

In present study, the single branch with stenosis was reconstructed for hemodynamics analysis and side branch were not included. Although side branches could introduce error to the hemodynamics of the stenotic artery, the impact was minor on the area of adverse hemodynamics [49]. Therefore, results of the present study had indicated the reliability of the geometric reconstructions and calculated fFFR. The sample size was small in this study, and findings of this study required further analysis to evaluate the usefulness and efficacy of our coronary vascular model for hemodynamic analysis of the stenotic artery.

V. CONCLUSION

In this paper, we have presented an alternative approach to determine FFR in stenotic coronary arteries, by employing fusion of CAG images and IVUS images to establish spatial geometric models, and to thereafter perform CFD simulation to calculate the values of fFFR, to evaluate the effects between the geometric parameters of the coronary lesion and the values of fFFR in stenosed coronary arteries. The calculated fFFR values were shown to have good correlation and agreement with the mFFR values. The values of fFFR were shown to decrease with the increase in severity of the stenosis. The curvature of lesion, the length of the stenosis and such like features had weak correlations with the fFFR values; however, the geometric characteristics of the stenosed coronary artery still need to be taken into account in the diagnosis and treatment of the lesion of coronary artery. Overall, we can state that our coronary vascular model has a promising medical application, based on the validation of our computation fFFR method with mFFR.

ACKNOWLEDGMENT

(Xiaoqing Wang and Changnong Peng contributed equally to this work.)

REFERENCES

[1] E. J. Benjamin *et al.*, "Heart disease and stroke statistics–2017 update: A report from the american heart association," *Circulation*, vol. 135, no. 10, pp. e146–e603, 2017.

[2] S. S. Kwon *et al.*, "A novel patient-specific model to compute coronary fractional flow reserve," *Prog. Biophys. Mol. Biol.*, vol. 116, no. 1, pp. 48–55, 2014.

[3] G. S. Mintz *et al.*, "Determinants and correlates of target lesion calcium in coronary artery disease: A clinical, angiographic and intravascular ultrasound study," *J. Amer. College Cardiol.*, vol. 29, no. 2, pp. 268–274, 1997.

[4] D.-H. Shin *et al.*, "TCT-564 effect of intravascular ultrasound–guided vs. Angiography-guided new-generation drug-eluting stent implantation; meta-analysis with individual patient-level data from 2,345 randomized patients," *J. Cardiovascular Interventions*, vol. 9, no. 21, pp. 2232–2239, 2016.

[5] T. Nishi *et al.*, "Comparison of 3-dimensional and 2-dimensional quantitative coronary angiography and intravascular ultrasound for functional assessment of coronary lesions," *J. Cardiol.*, vol. 69, no. 1, pp. 280–286, 2017.

[6] R. M. Cothren, R. Shekhar, E. M. Tuzcu, S. E. Nissen, J. F. Cornhill, and D. G. Vince, "Three-dimensional reconstruction of the coronary artery wall by image fusion of intravascular ultrasound and bi-plane angiography," *Int. J. Cardiac Imag.*, vol. 16, no. 2, pp. 69–85, 2000.

[7] S. Balocco, O. Basset, C. Cachard, and P. Delachartre, "Spatial anisotropic diffusion and local time correlation applied to segmentation of vessels in ultrasound image sequences," in *Proc. IEEE Symp. Ultrason.*, vol. 2, Oct. 2003, pp. 1549–1552.

[8] A. Wahle, S. C. Mitchell, M. E. Olszewski, R. M. Long, and M. Sonka, "Accurate visualization and quantification of coronary vasculature by 3D/4D fusion from biplane angiography and intravascular ultrasound," in *Proc. SPIE, Int. Soc. Opt. Eng.*, vol. 4158, 2001, pp. 144–155.

[9] H. T. Ma, H. Wang, C. Wang, and W. K. Hau, "3D reconstruction of coronary arteries using intravascular ultrasound (IVUS) and angiography," in *Proc. IEEE Int. Conf. IEEE Region 10 (TENCON)*, Oct. 2013, pp. 1–4.

[10] I. Hanson, M. Shoukfeh, and A. E. Abbas, "Fractional flow reserve," in *Interventional Cardiology Imaging: An Essential Guide*, A. E. Abbas, Ed. London, U.K.: Springer, 2015, pp. 107–120.

[11] K. Govindaraju, I. AnjumBadruddin, G. N. Viswanathan, S. V. Ramesh, and A. Badarudin, "Evaluation of functional severity of coronary artery disease and fluid dynamics' influence on hemodynamic parameters: A review," *Phys. Medica*, vol. 29, no. 3, pp. 225–232, 2013.

[12] N. P. Johnson *et al.*, "Continuum of vasodilator stress from rest to contrast medium to adenosine hyperemia for fractional flow reserve assessment," *JACC Cardiovascular Interventions*, vol. 9, no. 8, pp. 757–767, 2016.
[13] N. H. J. Pijls *et al.*, "Measurement of fractional flow reserve to assess the functional severity of coronary-artery stenoses," *New England J. Med.*, vol. 334, no. 26, pp. 1703–1708, 1996.
[14] L. Xin *et al.*, "Three-dimensional hemodynamics analysis of the circle of Willis in the patient-specific nonintegral arterial structures," *Biomech. Model. Mechanobiol.*, vol. 15, pp. 1439–1456, Dec. 2016.
[15] L. Xin *et al.*, "Functional assessment of the stenotic carotid artery by CFD-based pressure gradient evaluation," *Amer. J. Physiol. Heart Circulatory Physiol.*, vol. 311, no. 3, pp. H645–H653, 2016.
[16] O. Parodi *et al.*, "Patient-specific prediction of coronary plaque growth from CTA angiography: A multiscale model for plaque formation and progression," *IEEE Trans. Inf. Technol. Biomed.*, vol. 16, no. 5, pp. 952–965, Sep. 2012.
[17] W. Wijns, "The one-stop shop offering both coronary anatomy and myocardial perfusion: May well be opening soon, around the corner," *JACC Cardiovascular Imag.*, vol. 5, no. 11, pp. 1112–1114, 2012.
[18] Z. Jun-Mei *et al.*, "Simplified models of non-invasive fractional flow reserve based on CT images," *PLoS One*, vol. 11, no. 5, p. e0153070, 2016.
[19] J. K. Min, *et al.*, "Diagnostic accuracy of fractional flow reserve from anatomic CT angiography," *J. Amer. Med. Assoc.*, vol. 308, no. 12, pp. 1237–1245, 2012.
[20] C. K. Zarins, C. A. Taylor, and J. K. Min, "Computed fractional flow reserve (FFT_{CT}) derived from coronary CT angiography," *J. Cardiovascular Transl. Res.*, vol. 6, no. 5, pp. 708–714, 2013.
[21] B.-K. Koo *et al.*, "Cardiac imaging diagnosis of ischemia-causing coronary stenoses by noninvasive fractional flow reserve computed from coronary computed tomographic angiograms," *J. Amer. College Cardiol.*, vol. 58, no. 19, pp. 1989–1997, 2011.
[22] P. D. Morris *et al.*, "Virtual fractional flow reserve from coronary angiography: Modeling the significance of coronary lesions results from the VIRTU-1 (VIRTUal fractional flow reserve from coronary angiography) study," *JACC Cardiovascular Interventions*, vol. 6, no. 2, pp. 149–157, 2013.
[23] P. D. Morris, F. N. van de Vosse, P. V. Lawford, D. R. Hose, and J. P. Gunn, "'Virtual' (computed) fractional flow reserve: Current challenges and limitations," *JACC Cardiovascular Interventions*, vol. 8, no. 8, pp. 1009–1017, 2015.
[24] M. I. Papafaklis *et al.*, "Fast virtual functional assessment of intermediate coronary lesions using routine angiographic data and blood flow simulation in humans: Comparison with pressure wire–fractional flow reserve," *Eurointervention J. EuroPCR Collaboration Work. Group Interventional Cardiol. Eur. Soc. Cardiol.*, vol. 10, no. 5, pp. 574–583, 2014.
[25] C. M. Gibson *et al.*, "TIMI frame count: A quantitative method of assessing coronary artery flow," *Circulation*, vol. 93, no. 5, pp. 879–888, 1996.
[26] S. Tu *et al.*, "Fractional flow reserve calculation from 3-dimensional quantitative coronary angiography and TIMI frame count: A fast computer model to quantify the functional significance of moderately obstructed coronary arteries," *JACC Cardiovascular Interventions*, vol. 7, no. 7, pp. 768–777, 2014.
[27] S. A. M. Baert, W. J. Niessen, E. H. W. Meijering, A. F. Frangi, and M. A. Viergever, "Guide eire tracking during endovascular interventions," in *Medical Image Computing and Computer-Assisted Intervention*. Berlin, Germany: Springer, 2003, pp. 965–972.
[28] C. Doulaverakis *et al.*, "IVUSAngio tool: A publicly available software for fast and accurate 3D reconstruction of coronary arteries," *Comput. Biol. Med.*, vol. 43, no. 11, pp. 1793–1803, 2013.
[29] A. Wahle, G. P. M. Prause, S. C. DeJong, and M. Sonka, "Geometrically correct 3-D reconstruction of intravascular ultrasound images by fusion with biplane angiography-methods and validation," *IEEE Trans. Med. Imag.*, vol. 18, no. 8, pp. 686–699, Aug. 1999.
[30] M. Laban *et al.*, "ANGUS: A new approach to three-dimensional reconstruction of coronary vessels by combined use of angiography and intravascular ultrasound," in *Proc. Comput. Cardiol.*, Sep. 1995, pp. 325–328.
[31] F. Auricchio, M. Conti, C. Ferrazzano, and G. A. Sgueglia, "A simple framework to generate 3D patient-specific model of coronary artery bifurcation from single-plane angiographic images," *Comput. Biol. Med.*, vol. 44, no. 1, pp. 97–109, 2014.
[32] C. V. Bourantas *et al.*, "A method for 3D reconstruction of coronary arteries using biplane angiography and intravascular ultrasound images," *Comput. Med. Imag. Graph.*, vol. 29, no. 8, pp. 597–606, 2005.
[33] G. E. Ragkousis, N. Curzen, and N. W. Bressloff, "Patient specific stent malapposition in challenging anatomy: An FEA methodology to understand numerically the extent of malapposition of latest generation stents," in *Proc. ASME Summer Bioeng. Conf.*, 2013, p. V01AT12A004.
[34] G. E. Ragkousis, N. Curzen, and N. W. Bressloff, "Simulation of longitudinal stent deformation in a patient-specific coronary artery," *Med. Eng. Phys.*, vol. 36, no. 4, pp. 467–476, 2014.
[35] C. Bertolotti, V. Deplano, J. Fuseri, and P. Dupouy, "Numerical and experimental models of post-operative realistic flows in stenosed coronary bypasses," *J. Biomech.*, vol. 34, no. 8, pp. 1049–1064, 2001.
[36] B. Liu, "The influences of stenosis on the downstream flow pattern in curved arteries," *Med. Eng. Phys.*, vol. 29, no. 8, pp. 868–876, 2007.
[37] T. Chaichana, Z. Sun, and J. Jewkes, "Computation of hemodynamics in the left coronary artery with variable angulations," *J. Biomech.*, vol. 44, no. 10, pp. 1869–1878, 2011.
[38] H. Mohammadi and F. Bahramian, "Boundary conditions in simulation of stenosed coronary arteries," *Cardiovascular Eng.*, vol. 9, no. 3, pp. 83–91, 2009.
[39] *Comsol Multiphysics User's Guide, Version 5.0*, Comsol AB, Stockholm, Sweden, 2015.
[40] M. Prasad *et al.*, "Co-registration of angiography and intravascular ultrasound images through image-based device tracking," *Catheterization Cardiovascular Interventions*, vol. 88, no. 7, pp. 1077–1082, 2016.
[41] C. Peng *et al.*, "The impact of the geometric characteristics on the hemodynamics in the stenotic coronary artery," *PLoS One*, vol. 11, no. 6, p. e0157490, 2016.
[42] W. Wu *et al.*, "Noninvasive fractional flow reserve derived from coronary computed tomography angiography for identification of ischemic lesions: A systematic review and meta-analysis," *Sci. Rep.*, vol. 6, Jul. 2016, Art. no. 29409.
[43] A. Valencia and F. Solis, "Blood flow dynamics and arterial wall interaction in a saccular aneurysm model of the basilar artery," *Comput. Struct.*, vol. 84, no. 21, pp. 1326–1337, 2006.
[44] B.-K. Koo, "Physiologic evaluation of bifurcation lesions using fractional flow reserve," *J. Interventional Cardiol.*, vol. 22, no. 2, pp. 110–113, 2009.
[45] Y. Yang *et al.*, "Impact of spatial characteristics in the left stenotic coronary artery on the hemodynamics and visualization of 3D replica models," *Sci. Rep.*, vol. 7, no. 1, Nov. 2017, Art. no. 15452.
[46] S. Tu *et al.*, "Diagnostic accuracy of fast computational approaches to derive fractional flow reserve from diagnostic coronary angiography the international multicenter FAVOR pilot study," *JACC Cardiovascular Interventions*, vol. 9, no. 19, p. 2024, Oct. 2016.
[47] M. Tröbs *et al.*, "Comparison of fractional flow reserve based on computational fluid dynamics modeling using coronary angiographic vessel morphology versus invasively measured fractional flow reserve," *Amer. J. Cardiol.*, vol. 117, no. 1, pp. 29–35, 2016.
[48] C. A. Taylor, T. A. Fonte, and J. K. Min, "Computational fluid dynamics applied to cardiac computed tomography for noninvasive quantification of fractional flow reserve: Scientific basis," *J. Amer. College Cardiol.*, vol. 61, no. 22, pp. 2233–2241, 2013.
[49] S. Beier *et al.*, "Impact of bifurcation angle and other anatomical characteristics on blood flow—A computational study of non-stented and stented coronary arteries," *J. Biomech.*, vol. 49, no. 9, pp. 1570–1582, 2016.

XIAOQING WANG received the B.S. degree in medicine from the Wannan Medical College, Wuhu, Anhui, China, in 1996, and the master's degree in medicine from The First Affiliated Hospital, Sun Yat-sen University, Guangdong, China, in 2006. From 1996 to 2003, he involved in clinical practice and teaching in the Affiliated Hospital of Wannan Medical College. Since 2006, he involved in clinical practice with the Department of Cardiovascular, Shenzhen Sun Yat-Sen Cardiovascular Hospital.

His majority is internal medicine, and he is expertise in treatment for vascular disease, including intervention treatment for coronary artery disease and arrhythmia.

CHANGNONG PENG received the master's degree in medicine from Sun Yat-sen Medical University in 1992. He was involved in clinical practice with the Department of Cardiovascular for the last 30 years and advanced studies in Fuwai Hospital, China, and Deutsches Herzzentrum München, Germany.

His majority is diagnosis and treatment for cardiovascular diseases. He is expertise in the diagnosis of difficult cardiovascular cases, rescue of critical cases, therapy for arrhythmia by drugs, ablation and pacing, and interventional diagnosis for coronary arterial diseases.

Dr. Peng is a member of the Guangdong Institutes of the Coronary Intervention Committee and the Guangdong Cardiac Pacing and Electrophysiology Committee.

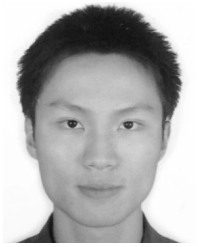

XIN LIU received the B.S. degree in biomedical engineering from the Guangdong Medical College, Guangdong, China, in 2009, and the M.S. degree in biomedical engineering from the University of New South Wales, Sydney, Australia, in 2011.

Since 2011, he has been a Research Assistant with the Shenzhen Institutes of Advance Technology, Chinese Academy of Sciences, Guangdong. His research interest includes the hemodynamic analysis of vascular disease base on arterial geometries reconstructed from medical images.

ZHIGENG PAN was born in 1965. He received the Ph.D. degree in engineering from Zhejiang University. His research interests include virtual reality, human–computer interaction, iconography, and digital entertainment.

He is the Secretary-General of the ACM SIGGRAPH Chinese Division, the Executive Director and a Deputy Secretary General of the Chinese Academy of Graphics, a Vice Director and a Secretary General of the China Image Graphics Society Virtual Reality Special Committee, a Deputy Director of the China Artificial Intelligence Society of Machine Perception and Virtual Reality and the Chinese Image Graphics Society Animation and Digital Entertainment Special Committee, and a member of the Editorial Board for the *International Journal of Image and Graphics* and the *International Journal of CAD/CAM*.